

EXPERIMENTAL IMPLEMENTATION OF THE MAXIMUM POWER POINT TRACKING ALGORITHM FOR A CONNECTED WIND TURBINE EMULATOR

ZOUHEYR DEKALI¹, LOTFI BAGHLI^{1,2}, ABDELMADJID BOUMEDIENE¹

Key words: Wind turbine emulator (WTE), Wind energy conversion system (WECS), Dc motor (DCM), Double fed induction generator (DFIG), Maximum power point tracking (MPPT), DS1104.

This paper presents the design, modeling and the experimental build of a 1.5 kW relatively low-cost wind turbine emulator (WTE) equipped by a DC motor (DCM) in order to simulate the static-dynamic behavior of a real wind turbine, including the gearbox. This emulator is integrated into a connected wind energy conversion system chain (WECS), based on the double fed induction generator (DFIG) configuration. The latter ensures the electromechanical conversion. It allows the transfer of active and reactive power with the power grid during hypo and hyper synchronous modes. The aerodynamic emulation principle requires controlling the DC armature current with a PI regulator. This leads to an electrical drive that applies a shaft torque identical to the wind turbine. The current reference is calculated as function of the static settings of the wind turbine and real wind speed data give different operating points. In addition, this paper also proposes to test the Tip Speed Ratio (TSR) based MPPT algorithm to extract the maximum available power on the emulator. The MPPT, the dc motor control and the DFIG power control algorithms are implemented in C, using dSPACE DS1104 control board. The experimental results confirm the effectiveness of the controlled dc motor to emulate the wind turbine with great performances of the proposed MPPT structure.

1. INTRODUCTION

In recent decades, looking for alternative energies has become very demanding, given the increased risk of excessive use of fossil fuels and their negative impact, on nature and human life [1,2]. According to the global wind energy congress GWEC, wind power is one of the fastest-growing renewable energy technologies, where the installed cumulative capacity exceeded 53.9 GW in 2018 in the global market. This is mainly due to its high techno-economic benefit and its renewable alternative source, environmentally friendly, as well as for solar energies [3].

Academic research in the renewable energy field considerably evolved, thanks to the great importance given by the energy policy of many governments around the world. The subject of this paper comes within the framework of the projects at the Laboratoire d'Automatique de Tlemcen (LAT) concerns the design, implementation and intelligent management of an energy production system which is composed of two wind turbine emulator (double fed induction generator (DFIG) and synchronous generator (SG)), and a photovoltaic system [4–7].

The main goal of this work is the development of a low-cost experimental bench for the emulation of a wind energy conversion chain based on a Double Fed Induction Generator (DFIG), with the use of a dc motor controlled in current for the mechanical emulation of a real wind turbine. This system manages several scenarios and operating points in both hyposynchronous and hypersynchronous modes. We can test different control laws (linear / non-linear) on both machines [8]. Thus, it is useable as an education tool for training and for PhD research at an affordable cost, in the field of renewable energy.

In the literature, the dc motor is the most chosen in the wind turbine hardware emulation for the mechanical inertia driving. Thanks to its linear model which ensures the

proportionality between the armature current and the torque, simple torque and speed control are easy to implement with enough precision and performance [9–11].

Currently, the Double Fed Induction Generator DFIG represents one of the best high techno-economic solutions for the wind power exploitation in most wind farms around the world [12]. It is less expensive compared to the synchronous machine. Moreover, it allows direct connection of the stator to the grid and the control of the power transfer by acting on the rotor currents using an inverter / rectifier connected to the rotor [13, 14].

This paper is organized as follows: We will first give in section II a detailed description of the overall proposed structure of this wind energy conversion system with a presentation of all the associated hardware elements of the experimental bench (machines, power electronic converters, measurements, software...). The static-dynamic modeling of the wind emulator, including the dc motor control algorithm with the TSR and the MPPT algorithm structure are discussed in section III. The experimental results and the interpretations are given in section IV. Finally, section V concludes the paper. YouTube videos related to the implementation and experiments can be found on [15].

2. EXPERIMENTAL HARDWARE DESCRIPTION

Figure 1 shows the overall structure of the experimental hardware of the wind turbine emulator, which is constituted of a dc motor of 1.5 kW mechanically coupled with the DFIG shaft, The DFIG stator is connected to the grid through an autotransformer TRT 8 A – 400 V 6 kVA for voltage adaptation and the transfer of the generated active and reactive power [16, 17]. The used power equipment consisting of a SEMIKRON Semiteach box which contain a6-IGBT's inverter with SKHI22 drivers that drives the DFIG rotor, this inverter is called the Machine Side Converter (MSC), that imposes the current references for

¹ LAT, Laboratoire d'Automatique de Tlemcen, Université de Tlemcen, 13000, Tlemcen, Algeria.

E-mails: zouheyr.dekali@univ-tlemcen.dz, abdelmadjid.boumediene@univ-tlemcen.dz

² GREEN, Groupe de Recherche en Électrotechnique et Électronique de Nancy, Université de Lorraine, EA 4366, Vandoeuvre-lès-Nancy, F-54500, France. E-mail: lotfi.baghli@univ-tlemcen.dz

reaching the desired DFIG active and reactive power using the rotor-flux vector control [4,9,18,19].

The Semiteach has also a diode-based 3-phases rectifier, which represents the point of divergence from other known grid connected DFIG based wind turbine structures, where IGBT's controlled rectifiers are used as a Grid Side Converter (GSC). In our application, for economic reasons, we minimize equipment costs. This allows us sharing the same dc bus for both the dc motor and the DFIG and using only one DSP control board to control both motors. Hence, when the induction machine is in hyper-synchronous speed operating mode, the rotor is generating active power and this power is absorbed by the chopper to drive the dc motor. The rectifier is connected to the grid through a second autotransformer TRT-13A 10 kVA.

Semiteach's fourth IGBT leg is used as a chopper for the dc motor control. The inverter has also filtering capacitors on the dc link and a big heat sinker.

To control both the DFIG and the dc motor, we use a dSPACE DS1104 single board control solution. It generates 7 PWM signals, 6 of them to control the 3-legs IGBT's grid side inverter to impose the DFIG rotor currents and one PWM signal for the dc chopper for imposing the calculated reference current. The Simple and Full PWM signals are issued by the TMS320F240 slave Digital Signal Controller of the dSPACE DS1104 board. In order to use this feature, we reprogrammed the firmware of the slave F240 DSC, leading to an optimum use of hardware and reducing the overall cost. We use the ADCs for the following measures: Two rotor phase currents and the dc motor current using LEM LA55 Hall effect sensors (I_{dr} , I_{qr} and I_{DCM} measurement) and two stator phase voltages and the dc bus voltage using LEM LV25-P Hall effect sensors (V_{sa} , V_{sb} and

U_{DC} measurement).

This uses 6 analog inputs over the 8 available ADC of the board, where 4 of them are multiplexed.

The mechanical speed and the rotor angle is measured thanks to an incremental encoder with the help of the index signal and interrupt service routine to compute the absolute position of the rotor.

The Control Desk™ running on the DS1104 host PC permits the visualization of the system variables in real time and the input of the reference values.

The main contribution of this paper concerns the improvement of a known MPPT which is applied to a grid-connected doubly fed induction generator (DFIG) used in wind energy conversion system (WECS) under different operating modes. We applied the tip speed ratio (TSR) control technique to extract the maximum power available on the drive train. We have validated our proposal thanks to experiments.

The novelty elements in this paper compared to other research is mainly the reduced cost of implementation of the experimental bench. We use just one dSPACE DS1104 control board to control both machines, and we use the same dc bus link between the rotor side of the DFIG and the dc motor. We have no use of back-to-back inverters thanks to that. In addition, this paper presents an overall analysis of a wind turbine energy conversion system, where we emphasis the machine control, power electronics, control algorithms ... etc. Furthermore, the study discusses the dynamic behaviors of the system, where we have modeled an aerodynamic system and we emulate it successfully. Rarely, we can find a simultaneous combination between the electrical and the mechanical part of the wind power system into one paper.

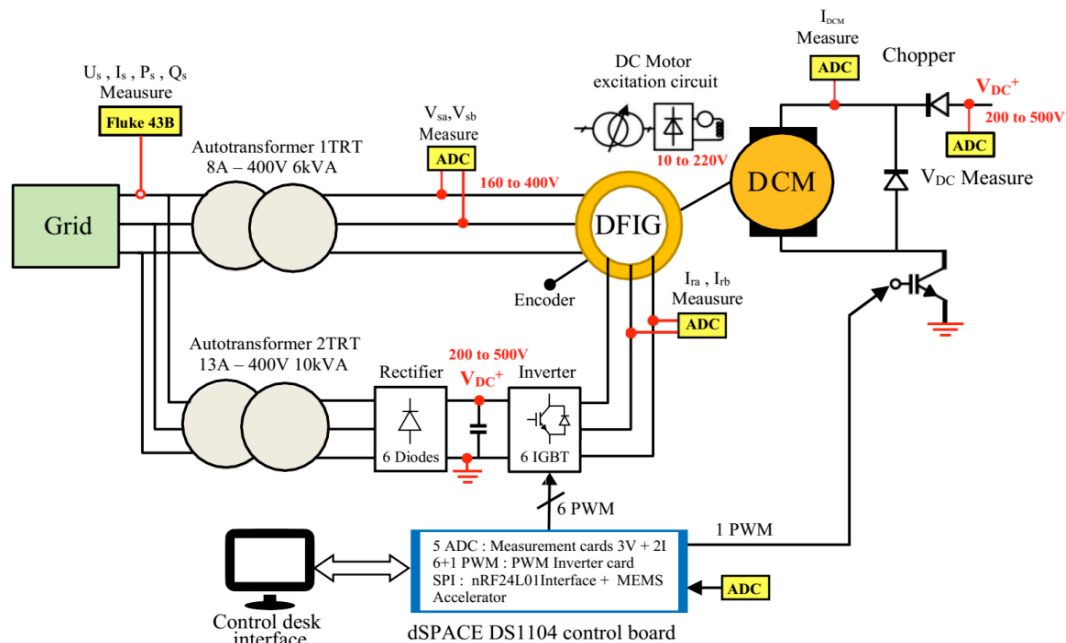


Fig. 1 – Experimental hardware structure of the wind turbine emulator.

3. WTE MODELING AND CONTROL

In this section, we will give the model of a fixed pitch wind turbine with horizontal axis, the static-dynamic model will be used to produce a dc motor torque identical to an aerodynamic torque at the steady-state conditions depends

on the wind speed and turbine characteristics. The wind turbine model can be divided into two parts [20,21]:

3.1. WIND TURBINE STATIC MODEL

The static model of the wind turbine is mainly characterized by the wind speed V , the blade pitch

angle β and the power coefficient C_p . The kinetic energy of wind captured by the blades in an air surface A transformed into mechanical energy is given by [22,23]:

$$P_m = \frac{1}{2} \rho A C_p V^3, \quad (1)$$

where $A = \pi R^2$ is the surface of the air column running through the turbine blades of a radius R , and ρ is the air density in (kg/m^3). The efficiency of each wind turbine is evaluated by the power coefficient value, this value depends mainly on the blade pitch angle β and the tip-speed ratio (TSR) λ . The power coefficient value is limited to 0.59, called Betz's limit. This theory states that a wind turbine can never convert more than 59 % of the kinetic energy contained in the wind into a mechanical energy. The commonly used approximation expression of the power coefficient C_p given as [22,24]:

$$C_p = 0.5176 \left(\frac{116}{\lambda_i} - 0.4\beta - 5 \right) \exp\left(\frac{-21}{\lambda_i} \right) + 0.0068\lambda, \quad (2)$$

with:

$$\frac{1}{\lambda_i} = \frac{1}{\lambda + 0.08\beta} - \frac{0.035}{\beta^3 + 1}. \quad (3)$$

The tip speed ratio λ is the ratio between the turbine mechanical speed Ω_t and the wind speed, is defined as [23]:

$$\lambda = \frac{\Omega_t R}{V}. \quad (4)$$

Figure 2 shows the variation of the power coefficient C_p as a function of the speed ratio λ , for some pitch angle values β . Each curve has its own maximum which corresponds to the maximum power that can be extracted from wind energy. This maximum is strongly influenced by the wind speed, since λ is a consequence of V . Therefore, variable speed wind turbines are more efficient than fixed speed wind turbines for extracting maximum power from wind [25].

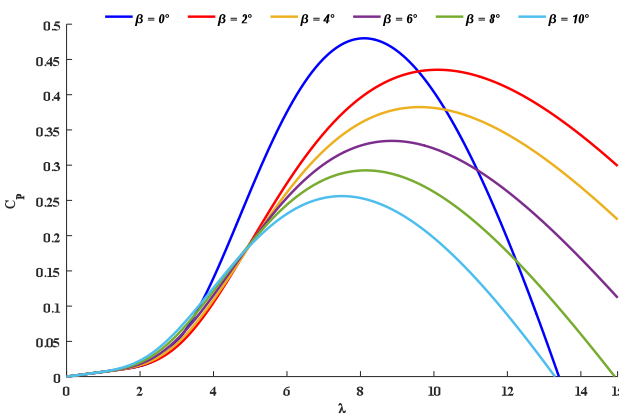


Fig. 2 – Power coefficient characteristics.

The aerodynamic torque available on the wind turbine shaft can be expressed as [14]:

$$T_t = \frac{1}{2\lambda} \rho A R C_p V^2. \quad (5)$$

3.2. WIND TURBINE DYNAMIC MODEL

Figure 3 illustrates the mechanical model of our WTE

system. It includes turbine blades and low speed shaft with inertia J_t , the gearbox, high speed shaft with inertia J_g and the electromechanical converter [21,26].

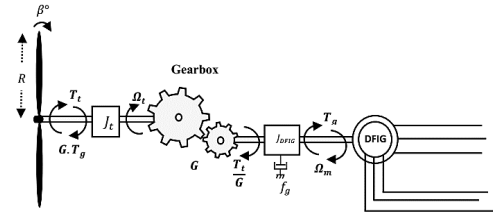


Fig. 3 – Mechanical model of a wind energy conversion system.

The fundamental mechanical equation of the system in the electrical generator side is giving as [27,28]:

$$\frac{T_t}{G} - T_g = J \frac{d\Omega_m}{dt}. \quad (6)$$

where T_t and T_g are the turbine torque and the DFIG torque respectively. The equivalent inertia J applied on the high-speed shaft (generator side) is expressed as [29,30]:

$$J = \frac{J_t}{G^2} + J_g. \quad (7)$$

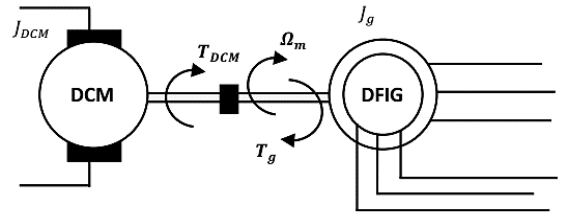


Fig. 4 – Mechanical model of the wind turbine emulator.

Figure 4 shows the mechanical model of the implanted emulator, including the opposing torques of the both machines applied on the common shaft with an equivalent inertia ($J_{DCM} + J_g$). The mechanical equivalent equation is expressed by [31]:

$$T_{DCM} - T_g = (J_{DCM} + J_g) \frac{d\Omega_m}{dt}. \quad (8)$$

with T_{DCM} : dc motor torque and T_g : DFIG torque (load torque for dc motor). The overall wind turbine static-dynamic model is assembled in (Fig. 5) [25,32].

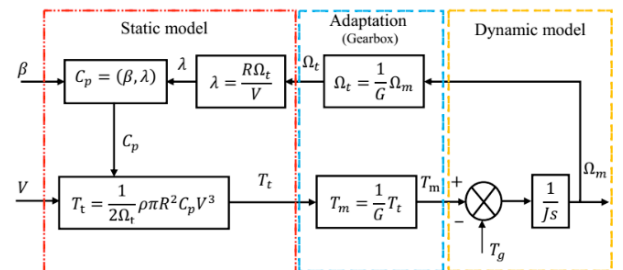


Fig. 5 – Overall wind turbine model.

3.3. THE PROPOSED WTE

The principle of emulation of a wind turbine is to create an aerodynamic torque from the dc motor. Figure 6 shows the proposed structure of the wind turbine emulator that is implanted at our laboratory [33]. The controlled dc motor

provides a variable output torque, which we consider equal to an adapted aerodynamic torque via an ideal gearbox [4,9,32].

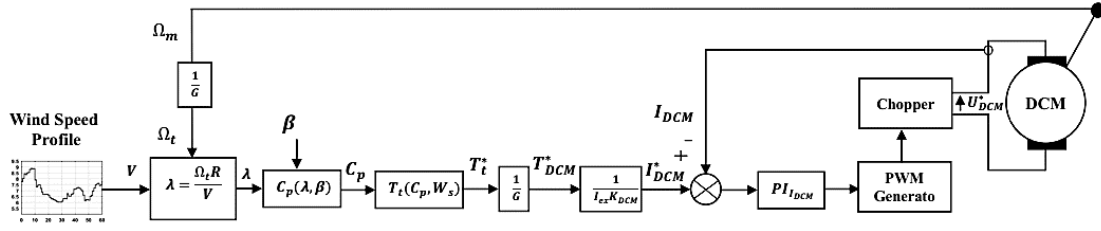


Fig. 6 – Overall diagram of the wind turbine emulator.

Equation (9) indicates the proportionality between the armature current and the dc motor torque [34]:

$$T_{DCM} = K I_{DCM}, \quad (9)$$

where K is the product of the electromotive force coefficient K_{DCM} and the excitation current I_{ex} . Therefore, while keeping this coefficient constant, controlling the torque, is done by acting on the armature current. The reference current I_{DCM}^* is calculated when applying a wind speed profile on the static-dynamic model of the wind turbine. Thus, the armature current follows the shape of the wind speed curve. So are the torque T_{DCM}^* and the supply voltage U_{DCM}^* . The calculated reference current is expressed as follows [35]:

$$I_{DCM}^* = \frac{\rho A}{2GK_{DCM} I_{ex}} \cdot \frac{C_p}{\Omega_m} \cdot V^3. \quad (10)$$

The proposed wind speed values interval allows testing transient of the transfer of the generated power between the power grid and the DFIG stator-rotor during operating modes: hyper synchronous, and hypo synchronous mode [18].

3.4. TSR BASED MPPT ALGORITHM STRUCTURE

Figure 7 Shows the WTE output mechanical power available on the DFIG-DCM common shaft at different wind speeds, therefore, the WTE rotational speed. The green line intersection points with the curves present the maximum power that needs to be extracted to achieve optimum operating point. Therefore, we apply TSR based MPPT algorithm to extract as much power as possible in the limited region colored with yellow, the interval of this limitation is chosen to be adaptable with the controller performances, also the hardware protection against overvoltage [36].

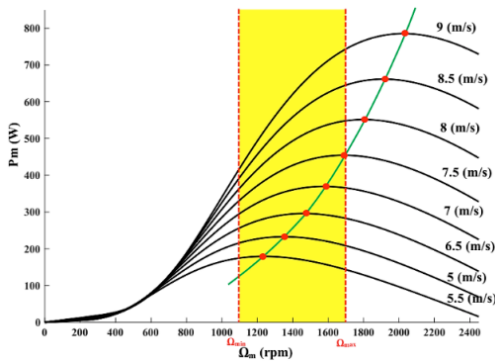


Fig. 7 – Overall WTE characteristic vs. rotational speed for different wind speeds.

The TSR structure is the most used MPPT algorithms, thanks to its efficiency and especially the simplicity of implementation. The principle is to keep the tip speed ratio

(TSR) to an optimum value λ_{opt} that corresponds the maximum of C_p (C_{pmax}) (Fig. 8), hence, the maximum of the extracted power. Therefore, it is necessary to maintain the WTE rotational speed at this operating point by adjusting the generator speed with a speed control loop [37,38].

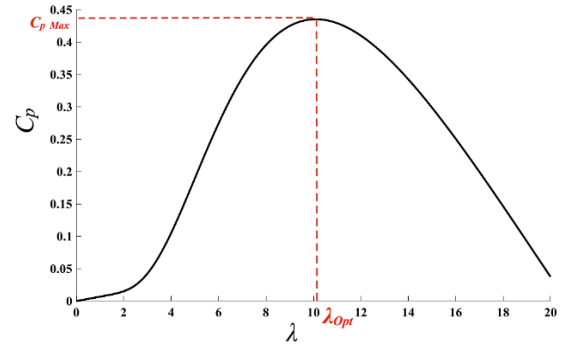


Fig. 8 –TSR principle based MPPT algorithm.

For our experimental emulator, we set β at 2° which corresponds to a maximum power coefficient C_{pmax} of 0.43 for an optimum tip speed ratio λ_{opt} of 10.22. Form eq. 4, the optimal speed reference is expressed as [25]:

$$\Omega_t^* = G \frac{\lambda_{opt} V}{R}. \quad (11)$$

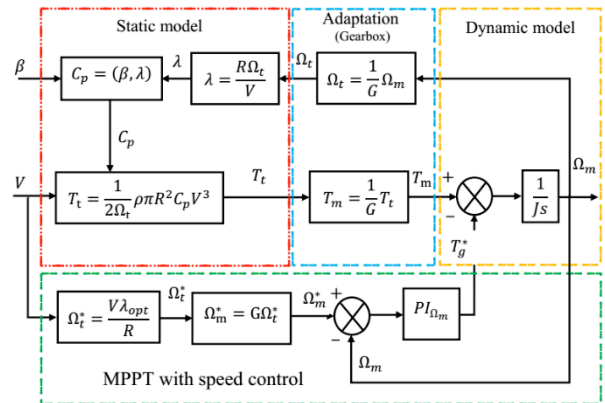


Fig. 9 –TSR based MPPT algorithm block diagram.

The block diagram of the TSR based MPPT algorithm is given by Fig. 9. The PI regulator is used to reduce the error between the optimal speed reference calculated in eq. (11) and the actual speed. This algorithm requires the accurate measurement of wind speed using an anemometer, this latter has an additive cost and it becomes a disadvantage for small turbine, add to that the inconvenience of the limited operating area [35,39].

4. EXPERIMENTAL RESULTS AND DISCUSSION

In order to validate the effectiveness of the proposed WECS structure, we conduct experimental tests. They consist of introducing different wind speed profiles that cover the operating modes. At every moment, the control applies a dc motor torque identical to the one of the emulated wind turbines, imposing the driving speed. In addition, the experiments test the MPPT efficiency by TSR method. We apply two tests:

First test: Figure 10 shows the results when slow reference changes of a wind profile between 5.5 and 8.5 m/s are applied to the system. The sinusoidal shape of the wind speed makes it possible to observe well the electro-mechanical phenomena of the WTE during the slow transition between the hypersynchronous towards the hypersynchronous, passing by the synchronous speed (1500 rpm) which correspond to a wind speed of 7 m/s (Fig. 10.a). We then get the WTE torques: turbine torque, which is adapted through the gearbox ratio to get a dc motor torque, they have the same form of the wind speed curve. Harmonic torques due to the gradient and tower

shadow effects are neglected and we consider the gearbox as ideal (Fig. 10.b). The tip speed ratio λ remains stable around its optimum value λ_{opt} (Fig. 10.c). The experimental value of the power coefficient C_p is around 0.42 (Fig. 10.d), which allows the production of a significant power. The WTE rotates at an optimum speed Ω_{opt} , that is adjusted perfectly by the speed control loop using PI controller (Fig. 10.e). The optimum reference speed Ω_{opt}^* is calculated by the MPPT algorithm based on the TSR structure. The latter show the capability to reach the maximum of the extracted power during the transition between the operating modes over a significant range (Fig. 10.i). A negative power means that it is injected to the grid. Figure 10.g shows the good tracking accuracy between the measured armature current I_{DCM} and the calculated reference I_{DCM}^* thanks to the PI current controller. The necessary dc motor voltage U_{DCM}^* that is outputted by the current controller is limited to 220 V for the protection of the dc motor (Fig. 10.h). When it reaches this limit, the current decreases inevitably. The active power high frequency fluctuations are due to the control of the rotor current components in Park reference frame (I_{dr} and I_{qr}) of the DFIG.

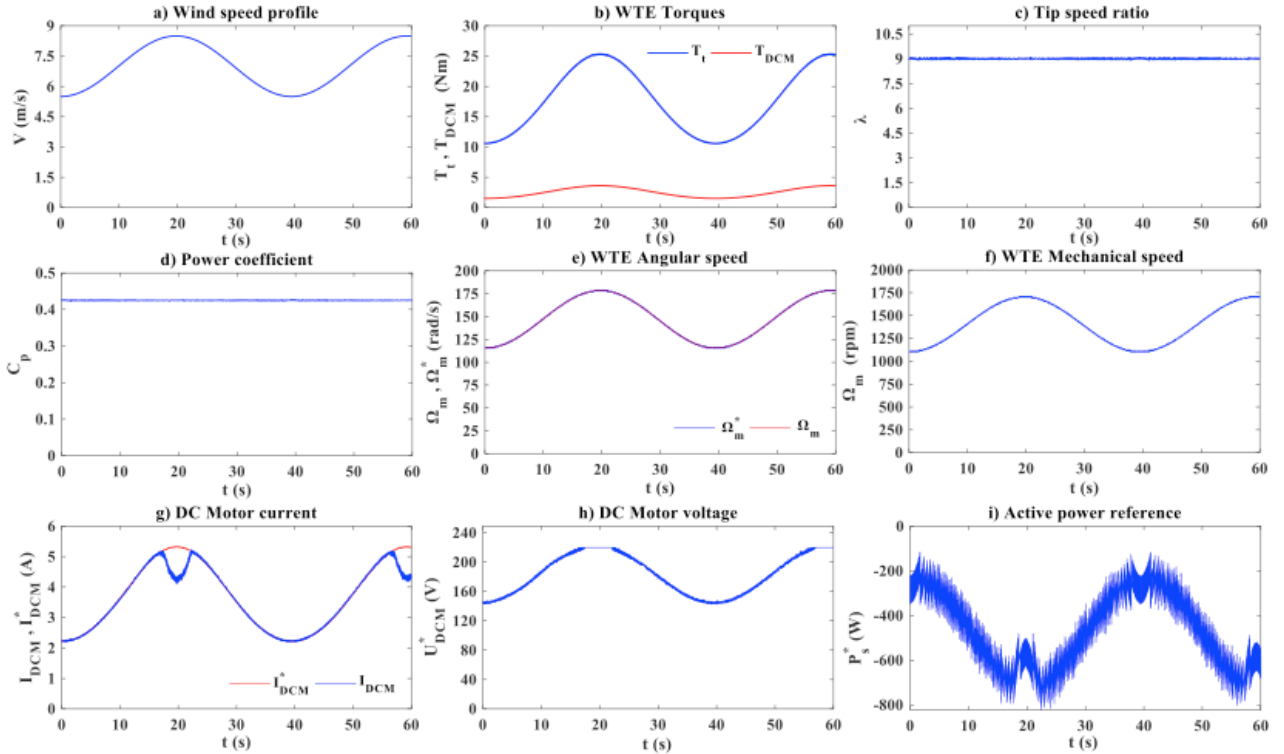
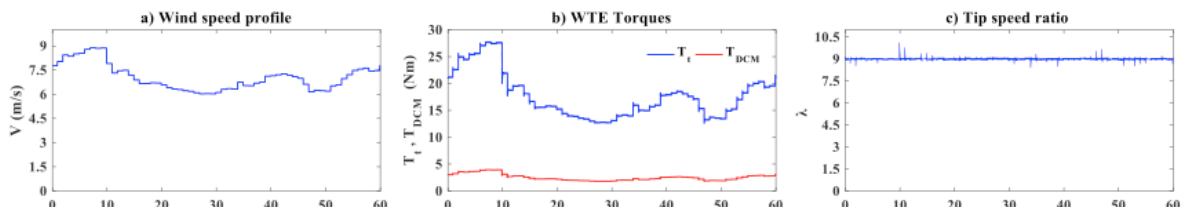


Fig. 10 – Experimental tests for a sinusoidal wind speed profile.

Second test: For this test, we have changed the wind speed reference; this time we apply a real wind speed profile to get closer to the actual behavior of a wind turbine power plant (Fig. 11.a). The resulting curves show the same dynamic performances of the WTE control as the previous experiment. The generated torques has a curve identical to that of the wind speed with negligible harmonics (Fig. 11.b). The spikes on the active power are due to high frequency noise from the measured rotor current. The low-

pass filter bandwidth is chosen wide to avoid any lag in the current measurement, but it let pass more hi-frequency contents (Fig. 11.i). These harmonics have little influence on the quality of the tip speed ratio curve (Fig. 11.c) and the power coefficient quality (Fig. 11.d). The control loop based on the numerical PI controller for the dc motor current shows high performances (Fig. 11.g), as well as the speed control loop (Fig. 11.e).



Concerning the experiments when the system is operating above synchronism, Fig. 10 and Fig. 11.a present this mode, when wind is above 7 m/s. Other subfigures show, over these periods, the behavior of the system and the production of power. So, over the same experiment, we have the different operating modes.

The starting process of the DFIG occurs normally. The stator is connected to the grid through an autotransformer. We increase the voltage until 200 V or 250 V and the DFIG get fluxed by consuming reactive power. The dc bus voltage is also set thanks to an autotransformer. Then we start the dc machine, and when the control synchronizes the DFIG to the grid (after 20 ms), we can start injecting active power and reactive power (e.g., compensate to PF = 1) by imposing references and thus Idr and Iqr (rotor currents) control the DFIG. We can choose different operating mode of the WTE: real wind data, sinusoidal variations, fixed wind, torque only: DCM current control or open loop: DCM voltage control.

5. CONCLUSIONS

A relatively low-cost wind energy conversion system was constructed successfully for an emulator test bench, with its associated power electronics and control system and program. The experimental results confirm the validity of the proposed WECS structure and its high performance by using a current controlled dc motor for the emulation of the wind turbine behaviors. On the other hand, the TSR based MPPT algorithm structure is very satisfactory for the extraction of the maximum power available. The DFIG control allows the injection of the active and reactive power to the grid.

This work allows the integration of this emulator in another test bench based on a synchronous generator and also for testing several linear and nonlinear control algorithms, either for educational use or for the development of research studies. According to national needs in MENA region, there is a need for training a new generation of engineers and researchers in the field of production of renewable energies.

Received on June 6, 2019

Appendix

Table 1
WTE Settings.

Setting	Parameter
Nominal power P_n	1.5 kW
Nominal speed	1500 rpm
Blade radius R	3 m
Gearbox ratio	7
Air density	1.225 kg/m ³

Table 2
WTE hardware component.

Component	Name
1	DFIG
2	DCM
3	PC
4	DS1104 interface
5	Inverter and Rectifier
6	Measure interfaces (DFIG)
7	Measure interfaces (DCM)
8	Autotransformer (stator side)
9	Autotransformer (rotor side)
10	Power supply (dc excitation)

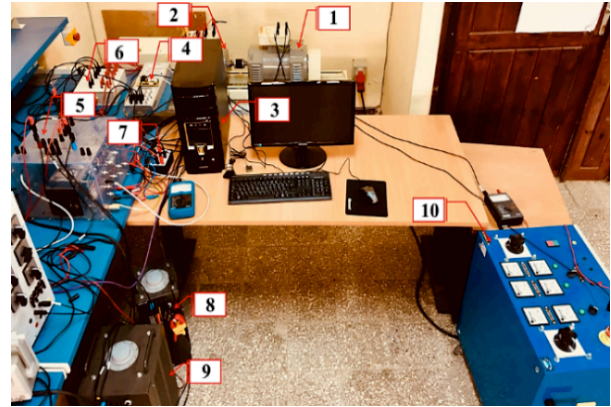


Fig. 12 – Experimental laboratory Setup.

REFERENCES

1. R. Ii. Ovando, J. Aguayo, M. Cotorogea, *Emulation of a low power wind turbine with a dc motor in matlab/simulink*, in 2007 IEEE Power Electronics Specialists Conference, Orlando, FL, USA, 2007.
2. A. Maafa, D. Aouzellag, K. Ghedamsi, R. Abdessemed, *Cascaded doubly fed induction generator with variable pitch control system*, Rev Roum. Sci. Tech.-Ser. Electrotech. Energ., **61**, 4, pp. 361–366 (2016).
3. Golbal Wind Report : *ANNUAL MARKET UPDATE 2017*. Global Wind Energy Council GWEC, 2017, [Online]. Available: <https://fr.slideshare.net/wyakab/gwec-global-wind-report-april-2018>.
4. L. Barote, C. Marinescu, I. Șerban, *Energy storage for a stand-alone wind energy conversion system*, Rev. Roum. Sci. Techn. – Électrotechn. Et Énerg., **55**, 3, pp. 235–242 (2010).
5. Z. Dekali, L. Baghli, A. Boumediene, *Experimental Implantation of an Emulator of a Wind Energy Conversion Chain System Based on Double Fed Induction Generator*, 11th Scientific Tech. Days Innov. Partnersh. Glob. CONTEXT ENERGY Transit., Oran, Algeria., Apr. 2018.
6. Z. Dekali, L. Baghli, A. Boumediene, *Control of a grid connected dfig based wind turbine emulator*, in 2018 5th Edition of the International Symposium, Environment-Friendly Energy and Applications (EFEA), Rome, Italy, 2018.
7. M. Merah and L. Baghli, *Simulation and comparison between conventional and interleaved buck-boost converter for grid-connected pv system*, SSRN Electron. J., 2018.
8. N. R. Averous et al., *Development of a 4 MW full-size wind-turbine test bench*, IEEE J. Emerg. Sel. Top. Power Electron., **5**, 2, pp. 600–609 (2017).
9. F. Amrane, A. Chaiba, B. E. Babes, S. Mekhilef, *Design and implementation of high performance field oriented control for grid-connected doubly fed induction generator via hysteresis rotor current controller*, Rev. Roum. Sci. Techn.– Électrotechn. et Énerg., **61**, 4, pp. 319–324 (2016).
10. S. Kouadria, S. Belfedhal, Y. Meslem, E. M. Berkouk, *Development of real time Wind Turbine Emulator based on dc motor controlled by hysteresis regulator*, in 2013 International Renewable and Sustainable Energy Conference (IRSEC), Ouarzazate, Mar. 2013.
11. L. A. Lopes, J. Lhuillier, M. F. Khokar, A. Mukherjee, *A wind turbine emulator that represents the dynamics of the wind turbine rotor and drive train*, in IEEE 36th Conference on Power Electronics Specialists, 2005., Aachen, Germany, 2005.
12. Yen Kheng Tan, S. K. Panda, *Optimized wind energy harvesting system using resistance emulator and active rectifier for wireless sensor nodes*, IEEE Trans. Power Electron., **26**, 1, pp. 38–50 (2011).
13. X. Dehong, B. Frede, C. Wenjie, Z. Nan, *Introduction: Advanced Control of Doubly Fed Induction Generator for Wind Power Systems*, Hoboken, NJ, USA: John Wiley & Sons, Inc., 2018, pp. 1–20.
14. X. Dehong, B. Frede, C. Wenjie, Z. Nan, *Basics of Wind Power Generation System: Advanced Control of Doubly Fed Induction Generator for Wind Power Systems*, Hoboken, NJ, USA: John Wiley & Sons, Inc., 2018, pp. 21–42.
15. L. Baghli, *GADA + émulateur de vent*. embesystems, 2018, [Online]. Available: <https://www.youtube.com/watch?v=gXJHaHWJdk0&t=17s>.
16. R. Nair, N. Gopalratnam, *Emulation of wind turbine system using vector-controlled induction motor drive*, IEEE Trans. Ind. Appl., pp. 1–1 (2020).
17. K. Schechner, C. M. Hackl, *Scaling of the drive train dynamics of large-scale wind turbine systems for real-time emulation in small-scale laboratory setups*, IEEE Trans. Ind. Electron., **66**, 9, pp.

- 6779–6788 (2019).
18. X. Dehong, B. Frede, C. Wenjie, Z. Nan, *DFIG Test Bench: Advanced Control of Doubly Fed Induction Generator for Wind Power Systems*, Hoboken, NJ, USA: John Wiley & Sons, Inc., 2018, pp. 21–42.
 19. M. Karabacak, L. M. Fernandez-Ramirez, T. Kamal, S. Kamal, *A new hill climbing maximum power tracking control for wind turbines with inertial effect compensation*, IEEE Trans. Ind. Electron., pp. 1–1 (2019).
 20. D. Llano, R. McMahon, M. Tatlow, *Control algorithms for permanent magnet generators evaluated on a wind turbine emulator test-rig*, in 7th IET International Conference on Power Electronics, Machines and Drives (PEMD 2014), Manchester, UK, 2014.
 21. A. Tohidi, H. Hajieghrary, M. A. Hsieh, *Adaptive disturbance rejection control scheme for dfig-based wind turbine: theory and experiments*, IEEE Trans. Ind. Appl., **52**, 3, pp. 2006–2015 (2016).
 22. M. Adjoudj, M. Abid, A. Aissouli, *Sliding mode control of a doubly fed induction generator for wind turbines*, Rev. Roum. Sci. Techn.–Électrotechn. et Énerg., **56**, 1, pp. 15–24 (2011).
 23. A. Asri, Y. Mihoub, S. Hassaine, P.O. Logerais, A. Amiar, T. Allaoui, *An adaptive proportional integral method for maximum power point tracking control of permanent magnet synchronous generator wind energy conversion system*, Rev. Roum. Sci. Techn.–Électrotechn. et Énerg., **63**, 3, pp. 320–325 (2018).
 24. G. Abad, Ed., *Doubly Fed Induction Machine: Modeling and Control for Wind Energy Generation*. Hoboken, NJ: IEEE Press, 2011.
 25. K. Boulaam, K. Boukhelifa, *Output power control of a variable wind energy conversion system*, Rev. Roum. Sci. Techn.–Électrotechn. et Énerg., **62**, 2, pp. 197–202 (2017).
 26. J. Castelló, J. M. Espí, R. García-Gil, *Development details and performance assessment of a Wind Turbine Emulator*, Renew. Energy, **86**, pp. 848–857 (2016).
 27. L. K. Gan, J. K. H. Shek, M. A. Mueller, *Modeling and characterization of downwind tower shadow effects using a wind turbine emulator*, IEEE Trans. Ind. Electron., **64**, 9, pp. 7087–7097 (2017).
 28. M. Yin, W. Li, C.Y. Chung, L. Zhou, Z. Chen, Y. Zou, *Optimal torque control based on effective tracking range for maximum power point tracking of wind turbines under varying wind conditions*, IET Renew. Power Gener., **11**, 4, pp. 501–510 (2017).
 29. R. Cardenas, R. Pena, *Sensorless Vector Control of induction machines for variable-speed wind energy applications*, IEEE Trans. Energy Convers., **19**, 1, pp. 196–205 (2004).
 30. X. Dehong, B. Frede, C. Wenjie, Z. Nan, *Modeling of DFIG Wind Power Systems: Advanced Control of Doubly Fed Induction Generator for Wind Power Systems*, Hoboken, NJ, USA: John Wiley & Sons, Inc., pp. 65–97.
 31. O. Barambones, J.A. Cortajarensidro, C. Jose, M.G de Durana, P. Alkorta, A.K. Mollae, *Variable speed wind turbine control scheme using a robust wind torque estimation*, Renew. Energy, **133**, pp. 354–366 (2019).
 32. J. M. Guerrero, C. Lumberras, D. D. Reigosa, P. Garcia, F. Briz, *Control and Emulation of small wind turbines using torque estimators*, IEEE Trans. Ind. Appl., **53**, 5, pp. 4863–4876 (2017).
 33. R. Azizpanah-Abarghooee, M. Malekpour, T. Dragicevic, F. Blaabjerg, V. Terzija, *A linear inertial response emulation for variable speed wind turbines*, IEEE Trans. Power Syst., **35**, 2, pp. 1198–1208 (2020).
 34. L. Benaouinate, M. Khafallah, A. Mesbahi, A. Martinez, *Development of a useful wind turbine emulator based on permanent magnet DC motor*, in 2017 14th International Multi-Conference on Systems, Signals & Devices (SSD), Marrakech, Mar. 2017.
 35. F. Martinez, L. C. Herrero, S. de Pablo, *Open loop wind turbine emulator*, Renew. Energy, **63**, pp. 212–221 (2014).
 36. F. Arevalo, P. Estrada, N. Pozo, M. Pozo, *Wind generation emulator using a DC machine*, in 2017 IEEE Second Ecuador Technical Chapters Meeting (ETCM), Salinas, Oct. 2017.
 37. Y. Zou, M. E. Elbuluk, Y. Sozer, *Stability analysis of maximum power point tracking (mppt) method in wind power systems*, IEEE Trans. Ind. Appl., **49**, 3, pp. 1129–1136 (2013).
 38. A. Mesbahi, M. Khafallah, A. Saad, A. Nouaiti, *Emulator design for a small wind turbine driving a self excited induction generator*, in 2017 International Conference on Electrical and Information Technologies (ICEIT), Rabat, Nov. 2017.
 39. D. Kumar, K. Chatterjee, *A review of conventional and advanced MPPT algorithms for wind energy systems*, Renew. Sustain. Energy Rev., **55**, pp. 957–970 (2016).